Eur. Phys. J. A **11**, 385–392 (2001)

THE EUROPEAN PHYSICAL JOURNAL A

The halo of the exotic nucleus ^{11}Li: a single Cooper pair

F. Barranco[1], P.F. Bortignon[2,3], R.A. Broglia[2,3,4,a], G. Colò[2,3], and E. Vigezzi[2,3,b]

[1] Escuela Superior de Ingenieros Industriales, Universidad de Sevilla, Camino de los Descubrimientos, 41092 Seville, Spain
[2] Department of Physics, University of Milan, via Celoria 16, 20133, Milan, Italy
[3] INFN, Sezione di Milano, Milan, Italy
[4] The Niels Bohr Institute, University of Copenhagen, Blegdamsvej 17, 2100 Copenhagen, Denmark

Received: 9 May 2001
Communicated by A. Molinari

Abstract. If neutrons are progressively added to a normal nucleus, the Pauli principle forces them into states of higher momentum. When the core becomes neutron saturated, the nucleus expels most of the wave function of the last neutrons outside to form a halo, which, because of its large size, can have a lower momentum. It is an open question how nature stabilizes such a fragile system and provides the glue needed to bind the halo neutrons to the core. Here, we show that this problem is similar to that of the instability of the normal state of an electron system at zero temperature solved by Cooper, a solution which is at the basis of BCS theory of superconductivity. By mimicking this approach using, aside from the bare nucleon-nucleon interaction, the long wavelength vibrations of the nucleus ^{11}Li, the paradigm of halo nuclei, as tailored glues of the least bound neutrons, we are able to obtain a unified and quantitative picture of the observed properties of ^{11}Li.

PACS. 21.10.-k Properties of nuclei; nuclear energy levels – 21.60.Ev Collective models – 21.60.Jz Hartree-Fock and random-phase approximations – 27.20.+n $6 \leq A \leq 19$

Aside from "dark matter" [1], atomic nuclei, little droplets made out of protons and neutrons 10 fm across [2], make up a sizable fraction of the present mass of the universe. Research into the structure of atomic nuclei concentrates largely on the limits of the nuclear stability [3], where new physics is expected to be, in particular at the limits of neutron and proton number defining the so-called drip lines, that is the *loci* in the chart of nuclides of the isotopes and isotones displaying the largest number of neutrons and of protons, respectively. The most exotic nuclei [4], first produced in the laboratory only few years ago, are those that lie just within the drip lines, on the edges of nuclear stability. Of these, the atomic nucleus $^{11}_{3}\mathrm{Li}_8$, containing 3 protons and 8 neutrons, is rightly the most famous and better studied and provides the cleanest example of halo nuclei to date [5–11].

In halo nuclei, some of the constituent neutrons or protons venture beyond the drop's surface and form a misty cloud or halo. Not surprisingly, these extended nuclei behave very differently from ordinary ("normal") nuclei lying along the stability valley in the chart of nuclides. In particular, they are larger than normal nuclei of the same mass number, and they interact with them with larger cross-sections as well. In the case of ^{11}Li, the last two neutrons are very weakly bound. Consequently, these neutrons need very little energy to move away from the nucleus. There they can remain in their "stratospheric" orbits, spreading out and forming a tenuous halo. If one neutron is taken away from ^{11}Li, a second neutron will come out immediately, leaving behind the core of the system, the ordinary nucleus ^{9}Li. This result testifies to the fact that pairing, the attraction correlating pairs between the least bound particles in a system, plays a central role in the stability of ^{11}Li.

It is well known that pairing can radically affect the properties of a many-body system. In metals, pairing between the electrons gives rise to superconductivity [12]. In a dilute neutron gas, pairing can influence the properties of neutron stars, cold remnants of fierce supernova explosions [13]. Acting on a liquid made out of atoms of the lighter isotope of helium ($^{3}_{2}\mathrm{He}_1$) it leads to superfluidity [14]. In nuclei, it controls almost every aspect of nuclear structure close to the ground state and determines, to a large extent, which nuclei are stable and which are not [2,15].

The basic experimental facts which characterize ^{11}Li and which are also of particular relevance in connection with pairing in this system are: a) $^{9}_{3}\mathrm{Li}_6$ and $^{11}_{3}\mathrm{Li}_8$ are bound systems, $^{10}_{3}\mathrm{Li}_7$ is not, b) the two-neutron separa-

[a] e-mail: broglia@mi.infn.it
[b] e-mail: vigezzi@mi.infn.it

tion energy in ^{11}Li is only $S_{2n} = 0.294 \pm 0.03$ MeV [7] as compared with values of 10 to 30 MeV in stable nuclei, c) ^{10}Li displays s- and p-wave resonances at low energy, their centroids lying within the energy range 0.1–0.25 MeV and 0.5–0.6 MeV, respectively [16], while these orbitals, in particular the $p_{1/2}$ level, are well bound in nuclei of the same mass lying along the stability valley, d) the mean-square radius of ^{11}Li, $\langle r^2\rangle^{1/2} = 3.55 \pm 0.10$ fm [17–19], is very large as compared to the value 2.32 ± 0.02 fm of the ^{9}Li core, and testifies to the fact that the neutron halo must have a large radius ($\approx$ 6–7 fm), e) the momentum distribution of the halo neutrons is found to be exceedingly narrow, its FWHM being equal to $\sigma_\perp = 48 \pm 10\,\mathrm{MeV}/c$ for the (perpendicular) distribution observed in the case of the break-up of ^{11}Li on ^{12}C, a value which is of the order of one fifth of that measured during the break-up of normal nuclei [6,7], f) the ground state of ^{11}Li is a mixture of configurations where the two halo nucleons move around the ^{9}Li core in s^2- and p^2-configurations with almost equal weight [20,21], the wave functions of the two-particle–like normal nuclei, although being strongly mixed are, as a rule, dominated by a single two-particle configuration.

Before discussing the sources of pairing correlations in ^{11}Li, we shall study the single-particle resonant spectrum of ^{10}Li. The basis of (bare) single-particle states used was determined by calculating the eigenvalues and eigenfunctions of a nucleon moving in the mean field of the ^{9}Li core, for which we have used a Saxon-Woods potential parametrized as in refs. [2,22] (cf. [2], Vol. **I**, eqs. (2-181), (2-182); [22], eq. (3.48)), leading to a depth $V = 51 - 30(N-Z)/A\,\mathrm{MeV} = 41\,\mathrm{MeV}$. The continuum states of this potential were calculated by solving the problem in a box of radius equal to 40 fm, chosen so as to make the results associated with ^{10}Li and ^{11}Li discussed below, stable. While mean-field theory predicts the orbital $p_{1/2}$ to be lower than the $s_{1/2}$ orbital (cf. fig. 1, I(a)), experimentally the situation is reversed. Similar parity inversions have been observed in other isotones of $^{10}_{3}\mathrm{Li}_7$, like, *e.g.* $^{11}_{4}\mathrm{Be}_7$. Shell model calculations testify to the fact that the effect of core excitation, in particular of quadrupole type, play a central role in this inversion [23] (cf. also [24]). In keeping with this result, we have studied the effect the coupling of the $p_{1/2}$ and $s_{1/2}$ orbitals of ^{10}Li to quadrupole vibrations of the ^{9}Li core has on the properties of the $(1/2^+)$ and $(1/2^-)$ states of this system (monopole and dipole vibrations display no low-lying strength and their coupling to the single-particle states of ^{10}Li lead to negligible contributions). The vibrational states of ^{9}Li were calculated by diagonalizing, in the random phase approximation (RPA), a multipole-multipole separable interaction taking into account the contributions arising from the excitation of particles into the continuum states. We adopted the self-consistent value for the coupling strength, because a calculation in the neighbor nucleus ^{10}Be yields good agreement with the experimentally known transition probability of the quadrupole low-lying vibrational state [25,26].

In the calculation of the renormalization effects of the single-particle resonances of ^{10}Li due to the coupling to vi-

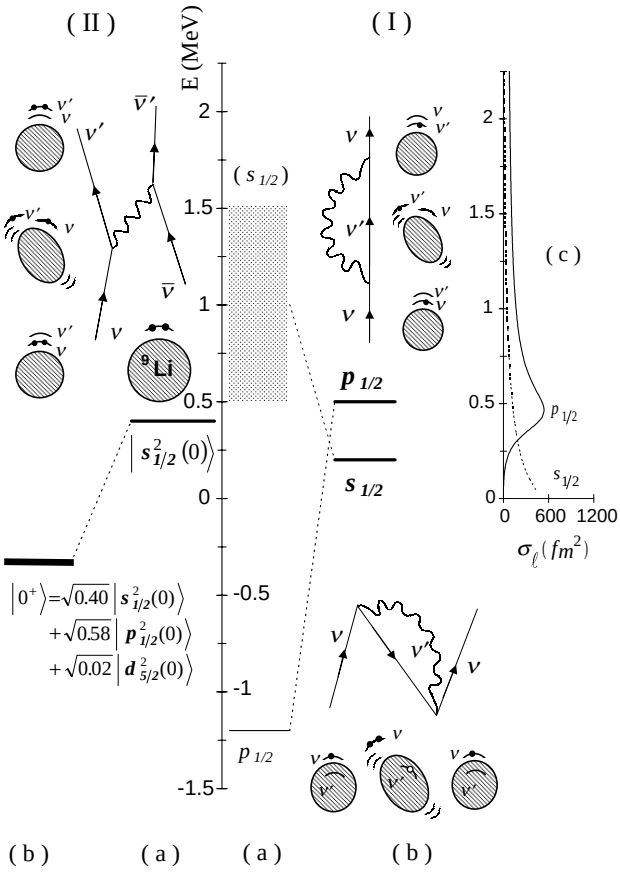

Fig. 1. (I) Single-particle neutron resonances in ^{10}Li. In (a) the position of the levels $s_{1/2}$ and $p_{1/2}$ calculated making use of mean-field theory is shown (hatched area and thin horizontal line, respectively). The coupling of a single-neutron (upward pointing arrowed line) to a vibration (wavy line) calculated making use of the Feynman diagrams displayed in (b) (schematically depicted also in terms of either solid dots (neutron) or open circles (neutron hole) moving in a single-particle level around or in the ^{9}Li core (hatched area)), leads to conspicuous shifts in the energy centroid of the $s_{1/2}$ and $p_{1/2}$ resonances (shown by thick horizontal lines) and eventually to an inversion in their sequence. In (c) we show the calculated partial cross-section σ_l for neutron elastic scattering off ^{9}Li. (II) The two-neutron system ^{11}Li. We show in (a) the mean-field picture of ^{11}Li, where two neutrons (solid dots) move in time-reversal states around the core ^{9}Li (hatched area) in the $s_{1/2}$ resonance leading to an unbound $s^2_{1/2}(0)$ state where the two neutrons are coupled to zero angular momentum. The exchange of vibrations between the two neutrons shown in the upper part of the figure leads to a density-dependent interaction which, added to the nucleon-nucleon interaction, correlates the two-neutron system leading to a bound state $|0^+\rangle$, where the two neutrons move with probability 0.40, 0.58 and 0.02 in the two-particle configurations $s^2_{1/2}(0)$, $p^2_{1/2}(0)$ and $d^2_{5/2}(0)$, respectively.

Table 1. RPA wave function of the collective low-lying quadrupole vibration of ^{9}Li (X and Y are the forwardsgoing and backwardsgoing amplitudes, respectively). The energy of this state is $E_{2+} = 3.3$ MeV. All the listed amplitudes refer to neutron transitions, except for the two last columns. We have adopted the self-consistent value ($\chi_2 = 0.013\,\mathrm{MeV}^{-1}$) for the coupling constant. The resulting value for the quadrupole transition probability corresponds to the deformation parameter $\beta_2 = 0.66$. A calculation of the low-lying quadrupole transition in the neighbouring nucleus ^{10}Be with the same coupling constant yields the value $\beta_2 = 0.9$, close to the experimental value $\beta_2 = 1.1$ [26].

	$1p^{-1}_{3/2}1p_{1/2}$	$1p^{-1}_{3/2}8f_{7/2}$	$1p^{-1}_{3/2}9f_{7/2}$	$1s^{-1}_{1/2}3d_{5/2}$	$1p^{-1}_{3/2}1p_{1/2}$ (π)	$1s^{-1}_{1/2}1d_{5/2}$ (π)
X_{ph}	1.02	0.07	0.08	0.07	0.15	0.09
Y_{ph}	0.28	0.05	0.06	0.06	0.09	0.07

brational states we have considered not only the effective-mass–like diagrams (upper-part graph of fig. 1, I(b)) leading to attractive (negative) contributions to the single-particle energies, but also those couplings leading to Pauli principle (repulsive) correction processes associated with diagrams containing two particles, one hole and a vibration in the intermediate states (lower-part diagram of fig. 1, I(b)). Because of such Pauli correction processes, the $p_{1/2}$ state experiences an upward shift in energy, arising from the coupling of this orbital to the $p_{3/2}$ hole state through quadrupole vibrational states, in keeping with the fact that the $(p_{1/2}p^{-1}_{3/2})$ particle-hole excitation constitutes an important component of the quadrupole vibration wave function (cf. table 1). As a consequence, the $p_{1/2}$ state becomes unbound, turning into a low-lying resonance with centroid $E_{\mathrm{res}} \approx 0.5$ MeV. Due to the coupling to the vibrations the s states are instead shifted downwards. In fact, in this case there are essentially no (repulsive) contributions arising from the Pauli correction processes. On the other hand, (attractive) effective-mass–like processes with intermediate states consisting of one particle plus a vibrational state of the type $(d_{5/2} \times 2^+)$ lead to a virtual state with $E_{\mathrm{virt}} = 0.2$ MeV (cf. fig. 1, I(b)). The above results provide an overall account of the s and p resonances observed experimentally. The important difference between the distribution of the single-particle strength associated with the resonant state $p_{1/2}$ and the virtual state $s_{1/2}$ can be observed in fig. 1, I(c), where the partial cross-section σ_l for neutron elastic scattering off ^{9}Li is shown. While σ_p displays a clear peak at 0.5 MeV, σ_s is a smoothly decreasing function of the energy. A small increase in the depth of the potential felt by the s-neutron will lead to a (slightly) bound state, hence the name of virtual (cf., *e.g.* [27]).

At the basis of the variety of pairing phenomena observed in systems so apparently different as atomic nuclei and metals is the formation of Cooper pairs [28,29]. In the case of metals, Cooper pairs arise from the combined effect of Pauli principle and of the exchange of lattice vibrations (phonons) between pairs of electrons (fermions) moving in time reversal states lying close to the Fermi energy. In the superconducting or BCS state of metals [12], Cooper pairs are strongly overlapping. In fact, there are on average 10^6 pairs which have their centers of mass falling within the extent of a given pair wave function. In spite of the modest number of Cooper pairs present in the ground state of atomic nuclei (≤ 10), BCS theory gives a quite accurate description of pairing in nuclei [2, 30], the analogy between the pairing gap typical of metallic superconductors and of atomic nuclei being very much to the point [31]. On the other hand, the finiteness of the nucleus introduces in the BCS treatment of pairing important modifications (quantal size effects (QSE), [30, 32–34]). In particular, while in the infinite system the existence of a bound state of the (Cooper) pair happens for an arbitrarily weak interaction [28], in the nuclear case this phenomenon takes place only if the strength of the nucleon-nucleon potential is larger than a critical value connected with the discreteness of the nuclear spectrum. In fact, calculations carried out making use of a particularly successful parametrization of the (bare) potential (Argonne potential [35]), show that the nuclear forces are able to bind Cooper pairs in open shell nuclei (leading to sizable pairing gaps (1-2 MeV) [36]), but not in closed shell nuclei, the most important contributions to the nucleon-nucleon (pairing) interaction arising from high multipole components of the force [30].

The situation is however quite different for the "open shell" nucleus ^{11}Li, as in this case the bare nucleon-nucleon interaction is not able to bind the two last neutrons to the ^{9}Li core. In fact, diagonalizing the Argonne potential in the basis of two-particle states $|nlj \times n'lj(0)\rangle$ coupled to angular momentum zero, does not lead to a bound state. The diagonalization was carried out by including all the two-particle configurations built out of the single-particle states with n' different or equal to n. The single-particle states are generated in a Woods-Saxon potential, with a depth associated to ^{11}Li, $V = 37.4\,\mathrm{MeV}(= 51 - 30(N - Z)/A$ MeV). Convergence of the results is obtained including single-particle levels with energy up to 150 MeV. The need for this high-energy cut-off, which in the case of ^{120}Sn becomes as large as 600 MeV (cf., *e.g.* [36]), is associated with the short-range repulsion of the Argonne potential (third term in the explicit expression given in [45]) which in the present case is dealt with explicitly and not in terms of a reduced space like, *e.g.*, in the case of Bruckner theory.

The low-lying states resulting from the diagonalization of the Argonne nucleon-nucleon force are essentially dominated by one of the configurations $|s^2_{1/2}(0)\rangle$, $|p^2_{1/2}(0)\rangle$ or $|d^2_{5/2}(0)\rangle$. In fact, the Argonne interaction produces almost no mixing between s-, p-waves and d-waves, but essentially it only shifts the energy of the unperturbed (res-

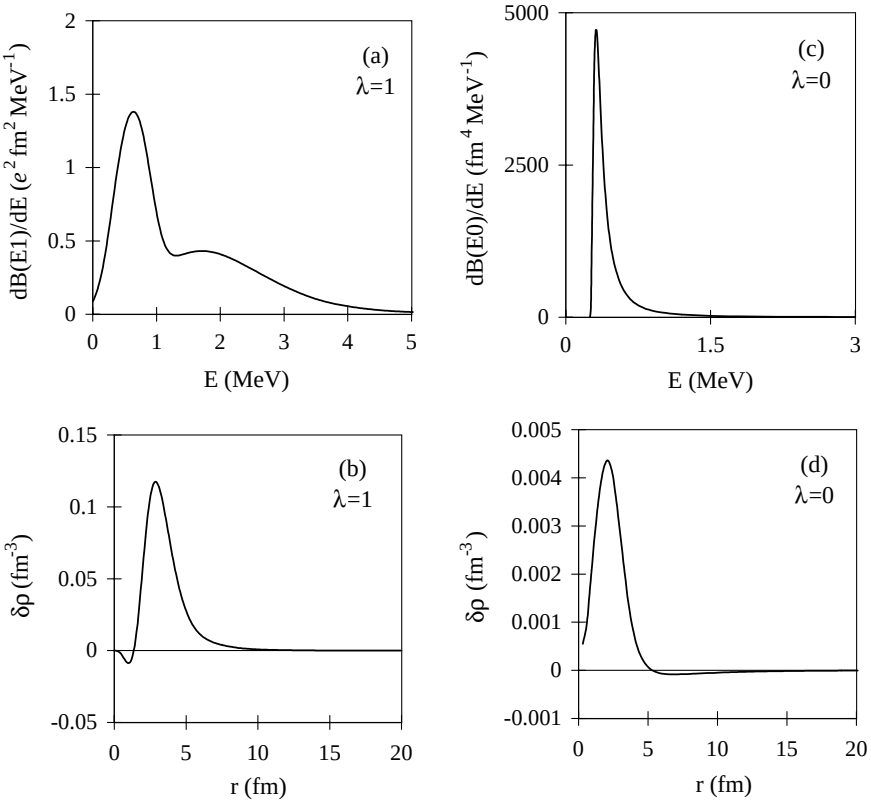

Fig. 2. Dipole and monopole linear response functions and transition densities of ^{11}Li calculated in the RPA. The dipole response ($J^\pi = 1^-$) was determined making use of the multipole-multipole separable interaction $H = t_z \chi_1 (F_1(\vec{r}_1) \cdot F_1(\vec{r}_2))_0$, with $F_{1M}(\vec{r}) = r \frac{\partial U}{\partial r} Y_{1M}$. The coupling constant was fixed so as to provide an overall account of the experimental findings [37, 38]. For simplicity we show in (a) the overall strength function (coarse mesh representation) and not the individual states (about 100). The transition density (b) is associated to the state close to the peak, at $E_{1-} = 0.75$ MeV. The associated wave function is displayed in table 3. No experimental information exists concerning the monopole modes. Consequently, an effective Skyrme interaction (SLy4) was used to determine the strength function shown in (c). The transition density at the peak ($E_{0+} \approx 0.5$ MeV) is shown in (d).

Table 2. RPA wave function of the collective low-lying quadrupole phonon in ^{11}Li, of energy $E_{2+} = 5.05$ MeV, and leading to the most important contribution to the induced interaction in fig. 1, II. All the listed amplitudes refer to neutron transitions, except for the last column. We have adopted the self-consistent value ($\chi_2 = 0.013\,\mathrm{MeV}^{-1}$) for the coupling constant. The resulting value for the deformation parameter is $\beta_2 = 0.5$.

	$1p^{-1}_{3/2}1p_{1/2}$	$2s^{-1}_{1/2}5d_{3/2}$	$1p^{-1}_{1/2}6p_{3/2}$	$2s^{-1}_{1/2}3d_{5/2}$	$2s^{-1}_{1/2}5d_{5/2}$	$1p^{-1}_{3/2}1p_{1/2}$ (π)
X_{ph}	0.824	0.404	0.151	0.125	0.126	0.16
Y_{ph}	0.119	0.011	−0.002	−0.049	−0.011	0.07

onant) configurations $s^2_{1/2}(0)$ and $p^2_{1/2}(0)$ by about 80 keV without giving rise to a bound system. To be noted that the $d^2_{5/2}(0)$ configurations are essentially not shifted. This result is very different from that obtained in nuclei lying around the stability valley where typical pairing correlation energies are of the order of 1.5 MeV. Making use of the same single-particle levels and of the same matrix elements of the nucleon-nucleon potential in connection with the BCS equations does not lead to a solution but to the trivial one of zero pairing gap ($\Delta_\nu = 0, U_\nu V_\nu = 0$) [30]. At the basis of this negative result is the fact, already mentioned above, that the most important single-particle states allowed to the halo neutrons of ^{11}Li to correlate are the $s_{1/2}$, $p_{1/2}$ and $d_{5/2}$ orbitals. Consequently the two neutrons are not able, in this low-angular momentum phase space, to profit from the strong force-pairing interaction, as essentially only the components of multipolarity $L = 0$, 1 and 2 of this force are effective in ^{11}Li because of angular momentum and parity conservation [39].

Because of this result and those of ref. [40], and in keeping with the fact that ^{11}Li displays low-lying collective vibrations [37,38], one can posit that the exchange of these vibrations between the two outer neutrons of ^{11}Li is likely to be the main source of pairing available to them to correlate. The $L = 0, 1$, and 2-vibrational spectra of ^{11}Li needed to calculate the matrix elements of this

Table 3. RPA wave function of the strongest low-lying dipole vibration of ^{11}Li, ($E_{1^-} = 0.75$ MeV), and contributing most importantly to the pairing induced interaction (fig. 1, II). All the listed amplitudes refer to neutron transitions. We have used the value $\chi_1 = 0.0043$ MeV^{-1} for the isovector coupling constant in order to get a good agreement with the experimental findings. To be noted that this value coincides within 25% close to the selfconsistent value of 0.0032 MeV^{-1}. The resulting strength function (cf. fig. 2(a)) integrated up to 4 MeV gives 7% of the Thomas-Reiche-Kuhn energy weighted sum rule, to be compared to the experimental value of 8% [38].

	$1p^{-1}_{1/2}2s_{1/2}$	$1p^{-1}_{1/2}3s_{1/2}$	$1p^{-1}_{1/2}4s_{1/2}$	$1p^{-1}_{1/2}1d_{3/2}$	$1p^{-1}_{3/2}5d_{5/2}$	$1p^{-1}_{3/2}6d_{5/2}$	$1p^{-1}_{3/2}7d_{5/2}$
$X_{\rm ph}$	0.847	−0.335	0.244	0.165	0.197	0.201	0.157
$Y_{\rm ph}$	0.088	0.060	0.088	0.008	0.165	0.173	0.138

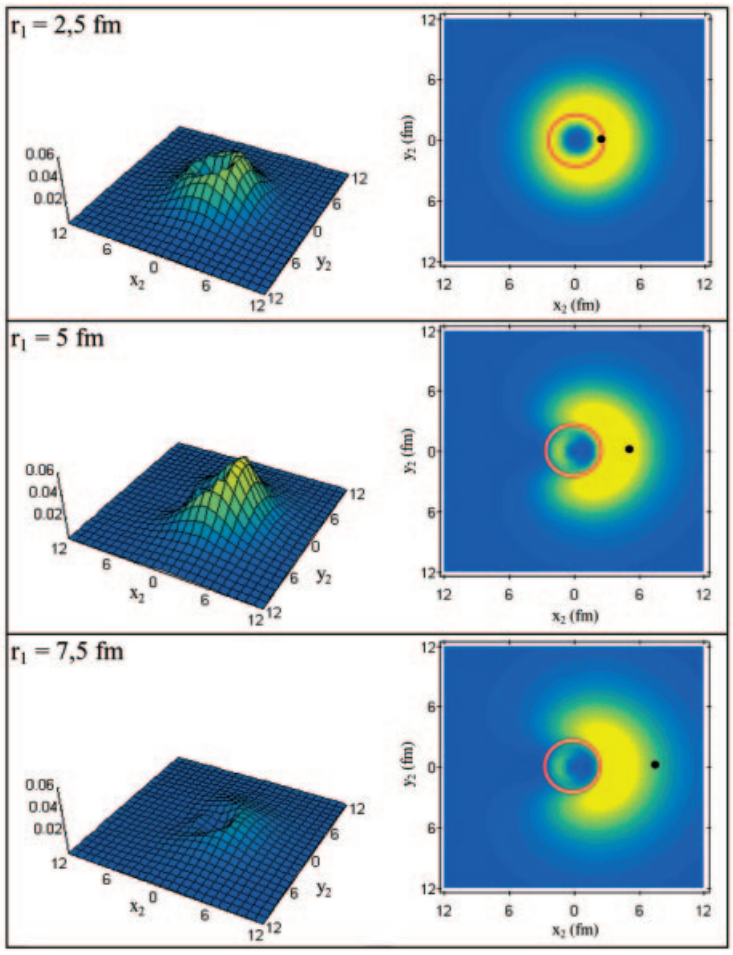

Fig. 3. Spatial structure of two-neutron Cooper pair. The modulus squared wave function $|\Psi_0(\vec{r}_1,\vec{r}_2)|^2 = |\langle \vec{r}_1,\vec{r}_2|0^+\rangle|^2$ (cf. fig. 2, II(b)) describing the motion of the two halo neutrons around the ^{9}Li core (normalized to unity and multiplied by $16\pi^2 r_1^2 r_2^2$) is displayed as a function of the cartesian coordinates $x_2 = r_2\cos(\theta_{12})$ and $y_2 = r_2\sin(\theta_{12})$ of particle 2, for fixed value of the position of particle 1 ($r_1 = 2.5, 5, 7.5$ fm) represented in the right panels by a solid dot, while the core ^{9}Li is shown as a red circle. The numbers appearing on the z-axis of the three-dimensional plots displayed on the left side of the figure are in units of fm^{-2}.

induced interaction were determined in much the same way as in ^{9}Li, that is, making use of the RPA. For the quadrupole coupling constant the same value used before was employed. Because the calculations have been carried out on the physical (correlated) ^{11}Li ground state, the particle-hole transitions associated with the vibrational states involving the $p_{1/2}$ and the $s_{1/2}$ states have been calculated with the energies and corresponding occupation numbers resulting from the full diagonalization. The strength of the separable dipole-dipole interaction has been adjusted so as to provide an overall account of the experimental dipole response in ^{11}Li [37,38]. Unperturbed particle-hole excitations up to 70 MeV have been included in the calculations and phonon states up to 50 MeV have been considered. Within this space there are of the order of 10^2 states, exhausting the associated energy-weighted

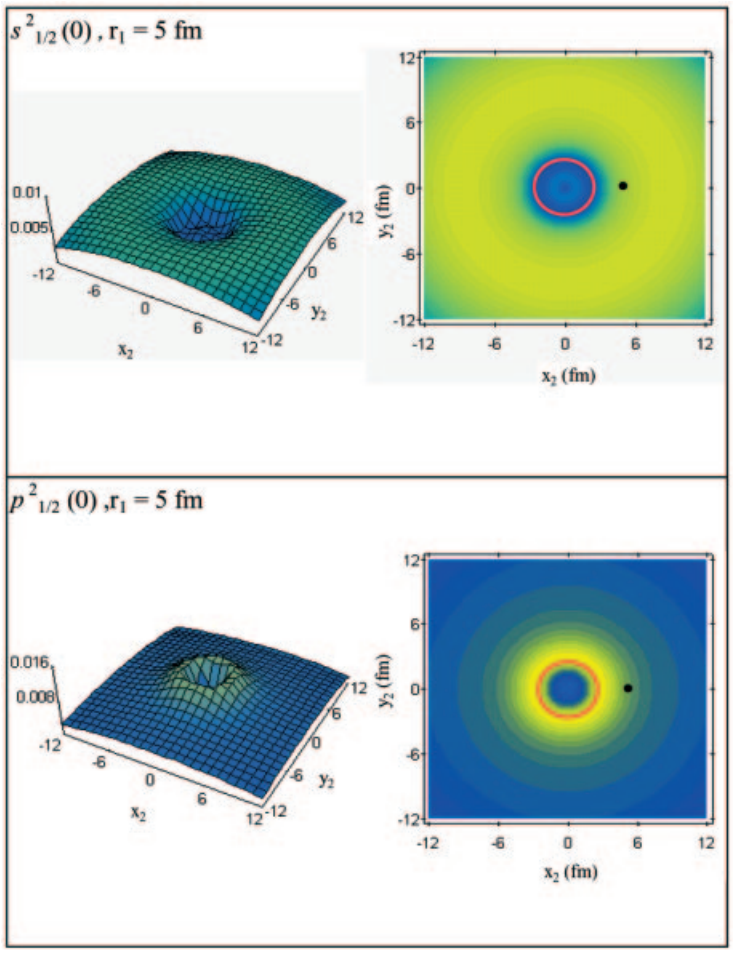

Fig. 4. Spatial distribution of the pure two-particle configurations $s^2_{1/2}(0)$ and $p^2_{1/2}(0)$ as a function of the x- and y-coordinates of particle 2, for a fixed value of the coordinate of particle 1 ($r_1 = 5$ fm). For more details cf. caption to fig. 3.

sum rule. The soft dipole response is shown in fig. 2(a). The low-lying quadrupole response is concentrated in a single peak, whose wave function is shown in table 2. A Skyrme-type effective interaction (SLy4) was instead used to calculate the monopole linear response. The corresponding solutions were obtained in coordinate space making use of a mesh extending up to a radius of 80 fm. The monopole response exhausts 94% of the EWSR considering the summed contributions up to 40 MeV of excitation energy (cf. fig. 2(c)).

All the resulting vibrational states were coupled to the single-particle states making use of the corresponding transition densities (form factors, cf. fig. 2(b) and 2(d)) and particle-vibration coupling strengths. In the monopole case, the response function was discretized in bins of 300 keV.

The calculations of the effects of the exchange of soft-dipole vibrational phonons includes the core dynamics in a fashion which is, to a large extent, equivalent to the calculations reported in ref. [41] within the framework of a three-body cluster model. In fact, in this model the soft dipole mode arises from the vibrations of the two weakly bound neutrons with respect to the ^{9}Li core. Within this model an interaction correlating the two neutrons arises from a cross term of the recoil kinetic energy of the core. In the Appendix to ref. [41] this term is shown to be equivalent to a separable dipole-dipole interaction of the type used in our calculations. To be noted however, that the cluster model does not include the renormalization effects of the single-particle motion (in particular s- and p-motion) arising from the coupling of single-particle motion to quadrupole vibrations of the ^{9}Li core. In fact, in the cluster model the core is assumed to be inert.

Allowing the two outer neutrons of ^{11}Li to both exchange phonons (induced interaction, fig. 1, II(a)), as well as to emit and later reabsorb them (self-energy correction, fig. 1, I(b)), leads to a bound (Cooper) pair, the lowest eigenstate of the associated secular matrix being $E_{\rm gs} = -0.270$ MeV. This result is mostly due to the exchange of the low-lying dipole vibrations shown in fig. 2(a) with associated wave function collected in table 3. Adding to the induced interaction the nucleon-nucleon Argonne potential, one obtains $E_{\rm gs} = -0.330$ MeV, and thus a two-neutron separation energy quite close to the experimental value. Measured from the unperturbed energy of a pair of neutrons in the lowest state calculated for

^{10}Li, namely the s resonance ($E_{\rm unp} = 2E_{s_{1/2}} = 400$ keV, cf. fig. 1, I(b)), it leads to a pairing correlation energy $E_0 = E_{\rm unp} - E_{\rm gs} = 0.730$ MeV (cf. fig. 1, II(b)). From the associated two-particle ground-state wave function $\Psi_0(\vec{r}_1, \vec{r}_2)(\equiv \langle \vec{r}_1, \vec{r}_2 | 0^+ \rangle)$, one obtains a momentum distribution (whose FWHM is $\sigma_\perp = 56$ MeV/c, for ^{11}Li on ^{12}C) and ground-state occupation probabilities of the two-particle states $s^2_{1/2}(0)$, $p^2_{1/2}(0)$ and $d^2_{5/2}(0)$ (0.40, 0.58 and 0.02 respectively, cf. fig. 1, II(b)) which provide an overall account of the experimental findings [42]. The radius of the associated single-particle distribution is 7.1 fm. Adding to this density that of the core nucleons, one obtains the total density of ^{11}Li. The associated mean-square radius (3.9 fm) is slightly larger than the experimental value.

The spatial structure of the Cooper pair described by the wave function $\Psi_0(\vec{r}_1, \vec{r}_2)$ is displayed in fig. 3. The mean-square radius of the center of mass of the two neutrons is $\langle r^2_{\rm cm} \rangle^{1/2} = 5.4$ fm. This result testifies to the importance correlations have in collecting the small (enhanced) amplitudes of the uncorrelated two-particle configuration $s^2_{1/2}(0)$ in the region between 4 to 5 fm, region in which the $p^2_{1/2}(0)$, helped by the centrifugal barrier, displays a somewhat larger concentration (cf. fig. 4). From the above results, it emerges that the exchange of vibrations between the least bound neutrons leads to a (density-dependent) pairing interaction acting essentially only outside the core (cf. also ref. [43]). To be noted that the long wavelength behaviour of these vibrations is connected with the excitation of the neutron halo, the large size of which not only makes the system easily polarizable but provides also the elastic medium through which the loosely bound neutrons exchange vibrations with each other [44].

The average mean-square distance between the halo neutrons is $\langle r^2_{12} \rangle^{1/2} \approx 9.2$ fm, in keeping with the fact that the coherence length [12] associated with Cooper pairs in nuclei is larger than the nuclear dimensions thus preventing the possibility of a nuclear supercurrent (cf., *e.g.* [2] Vol. **II**, p. 398). On the other hand, this value of $\langle r^2_{12} \rangle$ does not prevent the two correlated neutrons to be close together. The corresponding (small) probability (cf. fig. 3) being much larger than that associated with the uncorrelated neutrons (cf. fig. 4).

Similar results as those reported above are obtained solving the BCS equation for the two-neutron system making use of the matrix elements used in the diagonalization, sum of those of the nucleon-nucleon Argonne potential and those of the induced interaction. In this case, the correlation energy is $E_0 = 0.7$ MeV, the separation energy of the two neutrons becoming $S_{2\rm n} = 0.3$ MeV. The radial structure of the projected BCS wave functions $\sum_{\nu>0}(V_\nu/U_\nu)\varphi_\nu(\vec{r}_1)\varphi_\nu(\vec{r}_2)$ displays a spatial structure quite similar to $\Psi_0(\vec{r}_1, \vec{r}_2)$, the admixture of s- , p- and d-two particle configurations being now 46% and 51% and 3%, respectively. The coherence length ξ, that is the mean-square distance between the two neutrons forming the Cooper pair, is in this case, $\langle r^2_{12} \rangle^{1/2} = 7.8$ fm.

Arguably, the understanding of halo nuclei is the single, most important issue of nuclear structure research still awaiting a satisfactory explanation. We have shown that a substantial advance towards this goal is made by properly characterizing the role the surface of the system plays in renormalizing the bare nucleon-nucleon potential and the single-particle motion of the nucleons. In fact, we find compelling evidence which testifies to the fact that the mechanism which is at the basis of the presence of a low-density halo in ^{11}Li, is the coupling of weakly bound nucleons to long wavelength vibrations of the system leading to pairing instability and thus to a bound system. This result suggests a general strategy for designing nuclei with a large excess of neutrons or protons which may prove valuable in the current exploration of the drip line of the chart of nuclides, and thus in the design of new nuclear species: select those systems which display, under an increase of the excess of one type of nucleons, a marked softening of the long wavelength linear response. It is likely that such systems could venture far inside the region delimited by the drip lines, as the associated vibrational modes are expected to be an important source of (induced) pairing interaction, and thus to contribute significantly to the stability of the system.

We wish to thank G. Gori for technical help.

References

1. J.A. Peacock, *Cosmological Physics* (Cambridge University Press, Cambridge, 1999).
2. A. Bohr, B.R. Mottelson, *Nuclear Structure*, Vol. **I**, **II** (Benjamin, Reading, MA, 1969, 1975).
3. Y.T. Oganessian et al., Nature **400**, 242 (1999).
4. R.A. Broglia, P.G. Hansen (Editors), *Exotic Nuclei, 4th Course, International School of Heavy Ion Physics* (World Scientific, Singapore, 1998).
5. P.G. Hansen, A.S. Jensen, B. Jonson, Annu. Rev. Nucl. Part. Sci. **45**, 591 (1995).
6. T. Kobayashi et al., Nucl. Phys. A **553**, 465 (1993).
7. I. Tanihata, J. Phys. G **22**, 157 (1996).
8. R. Anne et al., Phys. Lett. B **250**, 19 (1990).
9. E. Arnold et al., Phys. Lett. B **281**, 16 (1992).
10. H. Esbensen, G.F. Bertsch, Nucl. Phys. A **542**, 310 (1992).
11. F. Barranco, E. Vigezzi, R.A. Broglia, Z. Phys. A **356** (1996) 45.
12. J.R. Schrieffer, *Theory of Superconductivity* (Benjamin, New York, 1964).
13. D. Pines, R. Tamagaki, S. Tsuruta (Editors), *The Structure and Evolution of Neutron Stars* (Addison-Wesley, Menlo Park, CA, 1992).
14. A. Leggett, in *The New Physics*, edited by P. Davies (Cambridge University Press, Cambridge, 1989) p. 268.
15. P. Walker, G. Dracoulis, Nature **399**, 35 (1999).
16. M. Zinser et al., Phys. Rev. Lett. **75**, 1719 (1995).
17. T. Kobayashi et al., Phys. Lett. B **232**, 51 (1989).
18. J.S. Al-Khalili, J.A. Tostevin, Phys. Rev. Lett. **76**, 3903 (1996).
19. P.G. Hansen, Nature **384**, 413 (1996).
20. N. Aoi et al., Nucl. Phys. A **616**, 181 (1997)c.

21. H. Simon et al., Phys. Rev. Lett. **83**, 496 (1999).
22. P.F. Bortignon, A. Bracco, R.A. Broglia, *Giant Resonances, Nuclear Structure at Finite Temperature* (Harwood Academic Press, Amsterdam, 1998).
23. H. Sagawa, B.A. Brown, H. Esbensen, Phys. Lett. B **309**, 1 (1993).
24. N. Vinh Mau, Nucl. Phys A **592**, 33 (1995).
25. F. Ajzenberg-Selove, Nucl. Phys. A **490**, 1 (1988).
26. S. Raman et al., At. Nucl. Data Tables **36**, 1 (1987).
27. L. Landau, E. Lifshitz, *Quantum Mechanics* (Pergamon Press, Oxford, 1965) p. 133.
28. L.N. Cooper, Phys. Rev. **104**, 1189 (1956).
29. J. Bardeen, L.N. Cooper, J.R. Schrieffer, Phys. Rev. **106**, 162 (1957); **108**, 1175 (1957).
30. S.T. Belyaev, Mat.-Fys. Medd. K. Dan. Vidensk. Selsk. **31**, no. 11 (1959).
31. A. Bohr, B.R. Mottelson, D. Pines, Phys. Rev. **110**, 936 (1958).
32. R. Kubo, J. Phys. Soc. Jap. **17**, 975 (1962).
33. R.H. Parmenter, Phys. Rev. **166**, 2490 (1968).
34. P.W. Anderson, J. Phys. Chem. Solids **11**, 26 (1959).
35. This nucleon-nucleon potential has been designed [45] so as to accurately reproduce the nucleon-nucleon phase shifts. It contains a number of terms which take into account isoscalar, isovector, spin-spin, tensor, spin-orbit, etc. interactions. The radial dependence of the force is composed of three terms of different ranges. In particular, the third term is related to the short-range repulsion typical of the strong force and associated with the exchange of ρ and ω mesons.
36. F. Barranco, R.A. Broglia, H. Esbensen, E. Vigezzi, Phys. Lett. B **390**, 13 (1996)
37. D. Sackett et al., Phys. Rev. C **48**, 118 (1993).
38. M. Zinser et al., Nucl. Phys. A **619**, 151 (1997).
39. This is the reason why the Cooper pair problem and the BCS treatment of pairing in the case of ^{11}Li looks (qualitatively) different from pairing in nuclei lying along the stability valley, and more similar to pairing in metals [12, 28], or even better in doped fullerides [46–48].
40. F. Barranco, R.A. Broglia, G. Gori, E. Vigezzi, P.F. Bortignon, J. Terasaki, Phys. Rev. Lett. **83**, 2147 (1999).
41. H. Esbensen, G.F. Bertsch, Phys. Rev. C **56**, 3054 (1997).
42. In ref. [49], the partial cross-section and corresponding momentum distributions have been studied in the one-neutron knockout reaction (^{12}Be, ^{11}Be + γ) on a ^{9}Be target. The reported experimental observation of about equal s- and p-spectroscopic factors is similar to the results found for the ground state of ^{11}Li in ref. [21]. The theoretical shell model analysis carried out with WBT matrix elements modified so as to reproduce the experimental findings predict a conspicuous $d^2_{5/2}(0)$ admixture, prediction which has not been experimentally tested, since knockout from this orbit leads to the unbound $(5/2^+)$ resonance in ^{11}Be which decays by neutrons. In any case, there are important differences between ^{11}Li and ^{12}Be, connected with the very different separation energies as well as with the dipole strength distribution which in ^{11}Li is much softer (enhanced low-energy behaviour) due to the higher polarizability of ^{11}Li as compared to ^{12}Be (cf. the recent experimental findings reported in ref. [50]).
43. G.F. Bertsch, H. Esbensen, Ann. Phys. (N.Y.) **209**, 327 (1991).
44. In keeping with the fact that the vibrational states of ^{11}Li are built out of excitations which occupy, to some extent, the same particle states occupied by the loosely bound neutrons we are studying, the corresponding particle-vibration matrix elements have been corrected from Pauli violating contributions following the nuclear field theory rules (cf. *e.g.* [2] and [51]). In particular, the reduction factors associated with the matrix elements $\langle s_{1/2} \times 1^- | H_{\rm c} | p_{1/2} \rangle$, $\langle s_{1/2} \times 0^+ | H_{\rm c} | s_{1/2} \rangle$ and $\langle p_{1/2} \times 0^+ | H_{\rm c} | p_{1/2} \rangle$ of the particle-vibration coupling Hamiltonian $H_{\rm c}$ the reduction factor are 2/3, 1/4 and 1/4, respectively.
45. R.B. Wiringa, R.A. Smith, T.L. Ainsworth, Phys. Rev. C **29**, 1207 (1984).
46. C.M. Lieber, Z. Zhang, Sol. State Phys. **48**, 349 (1994); W. Pickett, Sol. State Phys. **48**, 266 (1994).
47. M. Cotè et al., Phys. Rev. Lett. **81**, 697 (1998).
48. N. Breda, R.A. Broglia, G. Colò, G. Onida, D. Provasi, E. Vigezzi, Phys. Rev. B **62**, 130 (2000).
49. A. Navin et al., Phys. Rev. Lett. **85**, 266 (2000).
50. H. Iwasaki et al., Phys. Lett. B **491**, 8 (2000).
51. P.F. Bortignon, R.A. Broglia, D.R. Bes, R. Liotta, Phys. Rep. C **30**, 305 (1977).